Green Chemistry

PAPER

View Article Online
View Journal | View Issue

Cite this: *Green Chem.*, 2022, **24**, 7574

From haemoglobin to single-site hydrogenation catalyst†

Alain Y. Li,[a] Angus Pedersen,[a,b] Jingyu Feng,[a] Hui Luo,[a] Jesús Barrio,[a,b] Julien Roman,[a] King Kuok (Mimi) Hii[c] and Maria-Magdalena Titirici[*a,d]

Received 22nd June 2022,
Accepted 2nd September 2022

DOI: 10.1039/d2gc02344j

rsc.li/greenchem

Iron-based single-site catalysts hold immense potential for achieving highly selective chemical processes, with the added advantage of iron being an earth-abundant metal. They are widely explored in electrocatalysis for oxygen reduction and display promising catalytic activity for organic transformations. In particular, FeN_x@C catalysts are active for the reduction of nitroarene into aromatic amines. Yet, they are difficult to mass-produce, and most preparation methods fail to avoid single site aggregation. Here we prepared FeN_x@C catalysts from bio-derived compounds, xylose and haemoglobin, in a simple two-step process. Since haemoglobin naturally contains FeN_x single-sites, we successfully repurposed them into hydrogenation catalytic centers and avoided their aggregation during the preparation of the material. Their single-site nature was demonstrated by aberration-corrected transmission electron microscopy and X-ray absorption techniques. They were shown to be active for transfer hydrogenation of nitroarenes into anilines, with excellent substrate selectivity and recyclability, as demonstrated by the preserved yield across seven catalytic cycles. We also showed that FeN_x@C could be used to prepare 2-phenylbenzimidazole through a reduction/condensation tandem. Our work shows for the first time the viability of biomass precursors to prepare Fe single-site hydrogenation catalysts.

Introduction

Nitroarene reduction into aniline derivatives is the main method to obtain aromatic amines in the chemical industry.[1] Most processes rely on stoichiometric reduction using Fe^0/HCl (Béchamp process), or more commonly heterogeneous metallic hydrogenation catalysts (Pd, Ni Cu, Mn, or Fe).[2] Since Corma and Serna's breakthrough using Au/TiO_2,[3] a wide variety of nanocatalysts have been reported to date.[4] Additionally, in order to circumvent the use of flammable H_2 gas, alternative hydrogen donors such as iPrOH, HCO_2H, or silanes have been investigated. Indeed, many metals, ranging from precious metals (Au, Pt, Pd) to more abundant metals (Fe, Ni, Co) have been reported to be catalytically active in nitroarene transfer hydrogenation reactions.[5] Among these, Fe, while standing as the second most abundant transition metal in the earth crust, has emerged as a highly efficient catalyst.[6–10] Since the pioneering work of Beller and co-workers in using Fe-phenanthroline pyrolysed over carbon for nitroarene hydrogenation,[11–14] many nitrogen/carbon-supported Fe catalysts have since emerged (Fig. 1A).[14–18] In most reports, Fe was found as an ill-defined mixture of nanoparticulate species (metals, oxides, carbides and nitrides), without formal evidence of single sites. This mixture could lead to potential issues such as catalytic selectivity and metal leaching.

Single-site catalysts, with their well-defined atomic sites, can allow maximum metal usage while achieving high activity/selectivity.[19–22] There has been few examples of single-site FeN_x@C-catalysed hydrogenation: Cheong *et al.* reported a SBA-15-templated material, using $Fe(NO_3)_3$ and glucosamine as precursors, whereas Yun and Lu *et al.* opted for a MOF-encapsulated Fe precursor (Fig. 1B).[23–25] While all three catalysts were reported to be highly active and selective for nitroarene transfer hydrogenation reactions, the processes deployed highly carcinogenic hydrazine as a hydrogen source. In this work, we report a single-site FeN_x@C catalyst for highly-selective reduction of nitroarenes to anilines, using isopropanol as a hydrogen source.

In this work, the single-site catalyst FeN_x@C was prepared using haemoglobin as a bio-derived N/C precursor (Fig. 1C). As a waste product from the meat industry, haemoglobin contains a low Fe content (0.35 wt%) of FeN_4 heme units, which we

[a]*Department of Chemical Engineering, Imperial College London, Exhibition Road, London SW7 2AZ, UK. E-mail: m.titirici@imperial.ac.uk*
[b]*Department of Materials, Royal School of Mines, Imperial College London, Exhibition Road, London SW7 2AZ, England, UK*
[c]*Department of Chemistry, Imperial College London, Molecular Sciences Research Hub, 80, Wood Lane, London W12 0BZ, UK*
[d]*Advanced Institute for Materials Research (WPI-AIMR), Tohoku University, 2-1-1 Katahira, Aobaku, Sendai, Miyagi 980-8577, Japan*
† Electronic supplementary information (ESI) available. See DOI: https://doi.org/10.1039/d2gc02344j

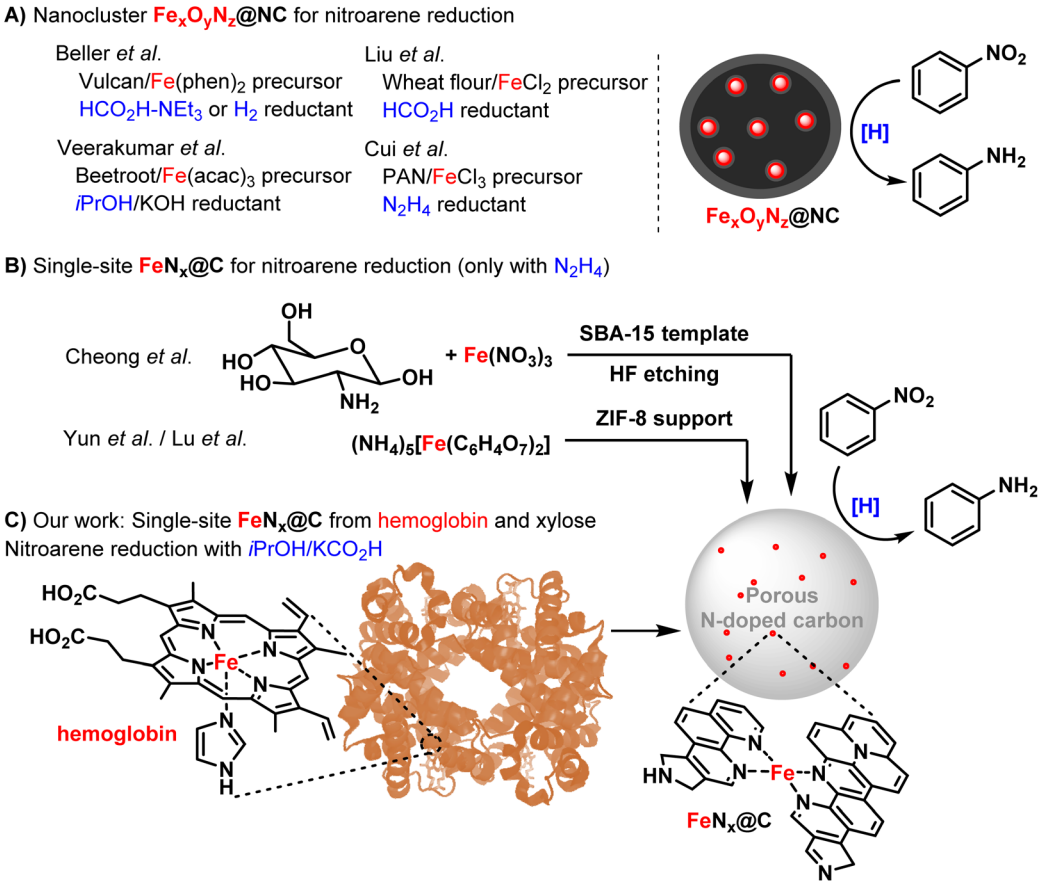

Fig. 1 Fe-Based catalysts for nitroarene reduction using (A) $Fe_xO_yN_z$ nanoclusters (B) using single-site FeN_x@C, and (C) our system using single-site FeN_x@C prepared from haemoglobin and using iPrOH/KCO_2H reductants.

repurposed into catalytic sites. It has been explored previously to prepare fuel cell cathode catalysts, by direct pyrolysis[26–31] or templated by $MgCl_2{\cdot}6H_2O$.[32,33] To the best of our knowledge, it has not been applied as a heterogeneous catalyst material. The present work will report a two-step preparation of a FeN_x@C catalyst, using only biomass starting materials derived from haemoglobin and xylose as a carbon source. The latter was selected due to its capacity as a C5 sugar to form polymerisable furans, and its availability from non-edible lignocellulosic biomass.[34]

Results and discussion

The catalyst was prepared in a two-step fashion (Scheme 1). Firstly, an aqueous solution of haemoglobin and xylose was subjected to hydrothermal carbonisation treatment (HTC) using kayexalate (poly(sodium 4-styrenesulfonate)) as a structure-directing agent.[35] HTC is a biomass carbonisation method, which entails the heating of aqueous solutions containing typically sugar-like molecules at 180–250 °C in a sealed autoclave.[36] The combination of heat and the autogenous

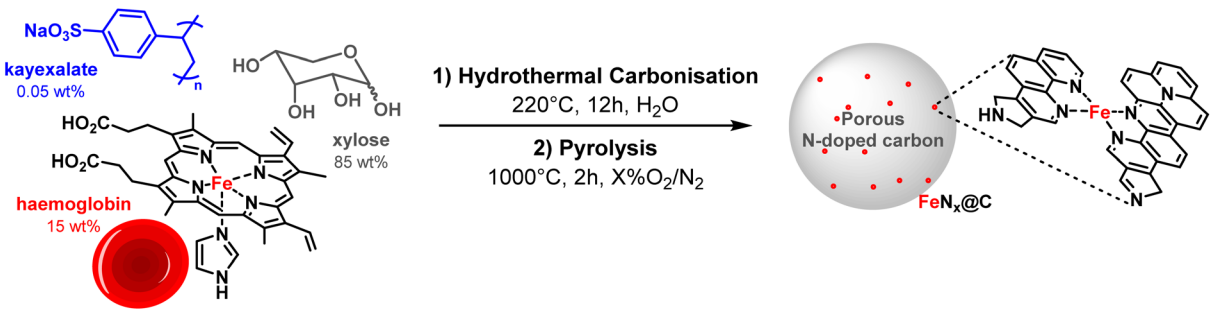

Scheme 1 Preparation of FeN_x@C.

pressure triggers sugar dehydration into furanic intermediates, followed by their polymerisation into carbon microspheres (2–5 μm).[37] This approach is based on a procedure developed previously within our research group, for the preparation of nitrogen-doped carbons from glucose and albumin protein.[38,39]

In a second step, the material obtained from HTC (named Fe_{HTC}) was thermally treated in a furnace under different atmospheres of varying oxygen/nitrogen ratios (0–10% O_2 in N_2). We measured the Fe concentration by ICP-MS through the catalyst preparation, showing that it increased from 580 ppm in the initial mixture to 1600 ppm after the HTC step, and to 2300–4000 ppm after pyrolysis depending on the oxygen content. The highest value (4000 ppm) was found at 6% oxygen. Throughout the HTC/pyrolysis sequence, we were able to increase the iron concentration relative to the other elements (C,N,O) from waste protein and biomass – while obtaining a nanoporous material.[40]

The preparation also resulted in an increase in the specific surface area of all the materials (from 40 $m^2\ g^{-1}$ for Fe_{HTC} to 70–740 $m^2\ g^{-1}$, Fig. 2A and Table S1†), with pores <5 nm in diameter (Fig. 2B). Conducting the synthesis of the catalyst without the template increased the specific area to 610 $m^2\ g^{-1}$ after pyrolysis.

Next, the catalytic activity of all of the prepared FeN_x@C samples was tested in the reduction of nitroarenes (Table 1). 4-Nitrotoluene was selected as a model substrate, using *i*PrOH both as a solvent and a reductant, in the presence of K_2CO_3 and KCO_2H as additives at 150 °C. While temperature conditions are considerably higher than for other single-site iron-based systems (25–60 °C), we strived to use safer reagents and solvents compared to the previous systems (comprising hydrazine, THF, NEt_3). Fe_{HTC}, and both the material treated with no template or no oxygen (Table 1, entries 1–3) were catalytically inactive (0% yield). With 2% oxygen thermal treatment, the yield increased to 7% (Table 1, entry 4), and increased to 56 and 75% yield at 4% and 6% oxygen treatment, respectively

Table 1 Catalyst screening for 4-nitrotoluene transfer hydrogenation

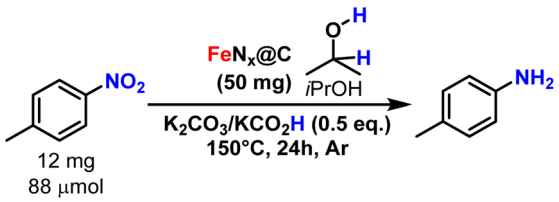

Entry	Catalyst	TOF (10^{-3} h^{-1})	Yield (%)
1	Fe_{HTC}	0	0
2	Same than FeN_x@C, without template	0	0
	Oxygen % during pyrolysis	**TOF (10^{-3} h^{-1})**	**Yield (%)**
3	0	0	0
4	2	82	7
5	4	719	56
6	6	770	75
7	8	249	20
8	10	111	1

Reaction conditions: 4-Nitrotoluene (12.4, 88 μmol), K_2CO_3 (6.1 mg, 0.5 equiv.), KCO_2H (3.7 mg, 0.5 equiv.), catalyst (50 mg), isopropyl alcohol (2.0 mL), Ar, 150 °C, 24 h.

(Table 1, entries 5 and 6). Upon further increasing the oxygen content to 8% and 10%, the yield decreased to 20 and 1% respectively (Table 1, entries 7 and 8). Thus, 6% oxygen treatment proved to be the most active catalyst, with a turnover frequency of 770 × 10^{-3} h^{-1} (assuming a full utilisation of the Fe atoms as single sites), in line with its higher BET specific surface area and highest Fe loading.

In Fig. 3 we have summarised the various parameters explored so far. We will thus keep the material at 6% oxygen throughout the rest of the manuscript, and refer to it as FeN_x@C.

X-ray Photoelectron Spectroscopy (XPS) showed a significant amount of surface oxygen (7.57 at%), along with 2.54 at% nitrogen and 0.05 at% Fe, the rest being carbon (analysis of

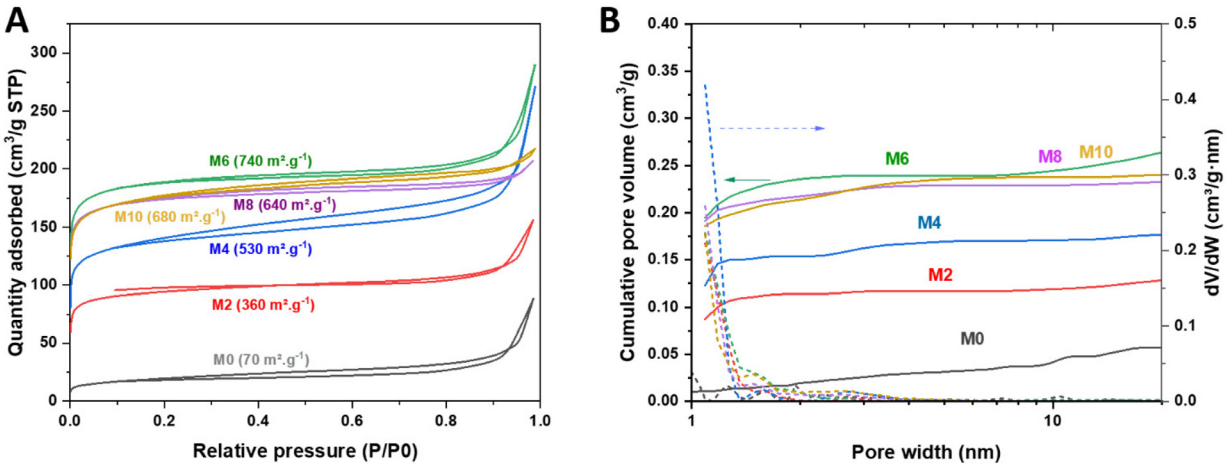

Fig. 2 (A) N_2 adsorption–desorption isotherm and (B) cumulative pore volume distributions for samples with different oxygen percentages during pyrolysis (the number after M indicates the oxygen percentage during pyrolysis).

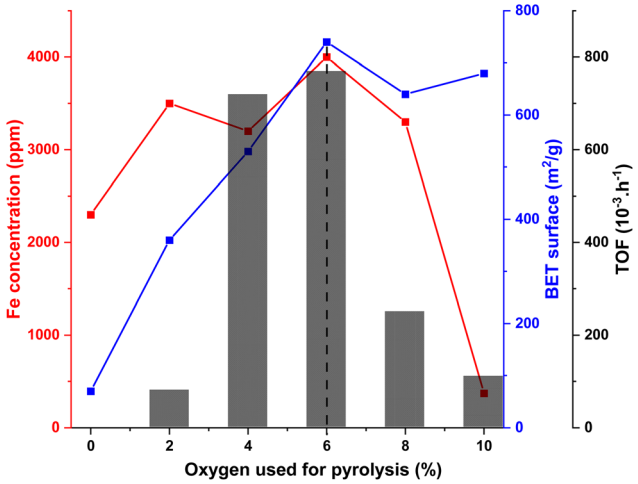

Fig. 3 Fe ICP-MS concentration, BET specific surface area and turnover frequency for the various materials prepared.

signals deconvolution is given Table S2 and Fig. S9 in ESI†). Raman and X-ray diffraction respectively showed that the carbon is amorphous (with an I_G/I_D ratio of 0.94), with no trace of crystalline iron oxide domain (Fig. S10 and S11†).

The single-site nature of FeN_x@C was then confirmed by means of electron microscopy (Fig. 4). SEM showed the spherical macrostructure of the carbon (2–10 μm, Fig. 4A and S8†). With TEM, no Fe particles were detected within the amorphous carbon matrix even at high magnification, excluding the presence of Fe species aggregates (Fig. 4B). Finally, aberration-corrected high resolution HAADF-STEM, showed sparse bright spots within the material (highlighted with red arrows), indicative of Fe single sites (Fig. 4C and D, Fig. S2–S4 in ESI†). More Fe single sites are embedded in the porous carbon matrix, which are difficult to image owing to the thickness of the carbon spheres.

Unlike for other FeN_x@C examples, no acid washing was required since no Fe-based nanocluster was detected by HAADF-STEM, XRD or X-ray absorption spectroscopy (XAS, *vide infra*). Indeed, the catalyst showed the same catalytic activity and Fe content with or without acid washing. We surmise that both the pre-coordination of Fe in heme sites along with their very low concentration contributed synergistically to avoid metal aggregation.[41]

Cryo (5K) X-band EPR was used to selectively probe Fe^{3+} sites within the catalyst, with potential Fe^{2+} and Fe^{4+} sites typically being EPR silent (Fig. 5).[42] The Fe precursor, haemoglobin, gives a clear signal at $g \sim 5.8$ and $g \sim 4.3$ which relates to high spin ($S = 5/2$) Fe in methaemoglobin and transferrin impurity, respectively. Additionally, a broad signal centered around $g \sim 2.1$ derives from ferritin, with this signal more evident at higher EPR temperatures. The sharp signal at $g = 2$ originates from organic radicals, with some potential contribution from the EPR tube or resonator. Interestingly, only a very small signal at $g \sim 4.3$ was found in the FeN_x@C catalyst, assigned to non-specifically bound high spin Fe^{3+} with large rhombic zero field splitting, possibly due to some leftover traces transferrin.[42,43] EPR sensitivity is typically in the order of μM,[44] while the Fe concentration in the catalyst is in the order of mM, suggesting Fe^{3+} in any significant proportion should be detected. Thus, the limited EPR response indicates that Fe exists almost entirely in the Fe^{2+} or Fe^{4+} state.

Having confirmed the single-site nature of FeN_x@C, we then investigated the role of each reaction component by conducting a series of control experiments (Table 2), starting with the use of base additives. In previous reports of both heterogeneous and homogeneous Fe catalysis, it has also been shown that the addition of a base helps activate the metal complex.[45,46] Typically, 1.0–5.0 equivalents of corrosive hydroxide salts (NaOH, KOH) are required. Only a few examples of base-free Fe catalysts have been reported for the transfer hydrogenation of nitroarenes ($Fe(BF_4)_2/HCO_2H$,[47] $FeBr_2/PhSiH_3$,[48] Fe_2O_3/HCO_2H[49]), but they all required costly phosphine ligands.

In our system, removing K_2CO_3 decreased the yield from 75% to 10% (Table 2, entry 1), showing the essential role of adding a base. Removing KCO_2H led to a similar conversion of the starting material (75%), but with half of the product being the hydrazine intermediate (34% of amine, 38% of 1,2-di-*p*-tolylhydrazine were formed, Table 2, entry 3). This shows that KCO_2H helps cleave the N–N bond of the hydrazine intermediate. Indeed, at no other point of the investigation this intermediate was detected when KCO_2H was present in the mixture. The indicates that the reduction occurs probably through the indirect nitroarene reduction pathway (see further details in ESI, Fig. S17 and S18†). As expected, the reaction did not proceed in the absence of catalyst, confirming the catalyst-base-reductant synergy (Table 2, entry 4). Substituting K_2CO_3 with Na_2CO_3 decreased the yield to 31%, in consistence with other reports on nitroarene transfer hydrogenation, with K_2CO_3 having a better solubility in alcohols (Table 2, entry 5).[50] KOH or NEt_3 decreased the yield to 36 and 16%, respectively (Table 2, entries 6 and 7). Replacing KCO_2H with NH_4CO_2H gave no yield (Table 2, entry 8), although some product was detected upon increasing the amount of NH_4CO_2H to 1 and 1.5 equivalents (23 and 25% yield, Table 2, entries 9 and 10). Finally, we used different Fe salts directly as catalysts in our optimal conditions. Fe^{3+} sources, such as Fe $(acac)_3$ and $FeCl_3$, were inactive for the reaction (Table 2, entries 11 and 12), while $FeCl_2$ gave a 14% yield, hinting at Fe^{2+} as the active species (Table 2, entry 13). Iron(II) phthalocyanine (FePc, Table 2, entry 14) was catalytically inactive, although this could be attributed to it being insoluble in iPrOH.[51] In comparison, a low level of catalytic activity was observed using the pure haemoglobin precursor (6% yield, Table 2, entry 15). Due to the chemical complexity of the precursor, we cannot exclude that its catalytic activity comes from the residual ferritin or the transferrin impurity in the sample (*vide supra* for the EPR analysis).

Next, the catalytic study was extended to other nitroarene substrates (Table 3). We first investigated steric hindrance surrounding the – nitro group. In comparison with the 85% yield

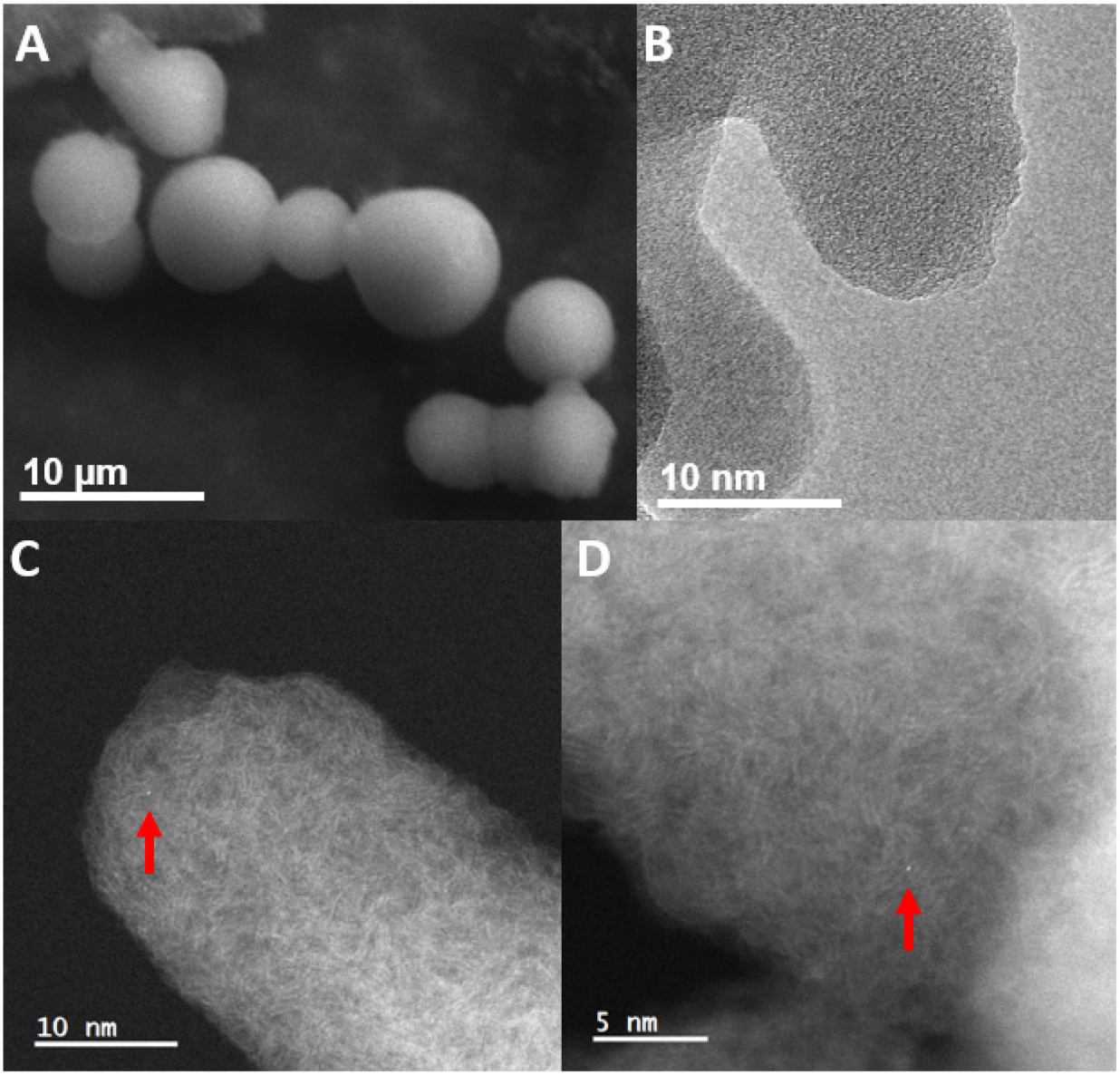

Fig. 4 (A) SEM image (B) TEM image (C) and (D) HAADF-STEM images of FeN_x@C (6% oxygen treatment, single site Fe are indicated with a red arrow).

obtained in the reduction of nitrobenzene (Table 3, entry 2), more sterically hindered substrates such as 2-ethylnitrobenzene or 1,3-dimethyl-2-nitrobenzene required a slightly increased Fe loading (5 mol%) to maintain high yields (69 and 77%, Table 3, entries 3 and 4). This is consistent with the predominantly nanoporous nature of the catalyst, making the catalytic site more difficult to access for bulkier substrates.

Chemoselectivity is a major challenge in nitroarene reduction,[52] since hydrogenation catalysts can also cleave weak bonds (such as carbon–halogen bonds), or reduce unsaturated bonds (C=C, C=O). Therefore, bifunctional nitroarenes bearing cleavable bonds or reducible groups were also included in the substrate study. The C–O ether bond in 1,2-(methylenedioxy)-4-nitrobenzene was preserved while keeping a high yield (85%, Table 3, entry 5). Although yields were lower, 4-iodonitrobenzene and 1,2,3-trichloro-5-nitrobenzene were successfully reduced while fully preserving the C–I and C–Cl bonds (58 and 46%, Table 3, entries 6 and 7). As for nitroanilines, the three isomers were reduced in high yields (97, 93 and 53%, Table 3, entries 8–10). Similarly, C=C, C≡C, C≡N bonds remained unaffected: 3-nitrostyrene gave a 71% yield (Table 3, entry 11), whereas 4-nitrobenzonitrile and 1-ethynyl-4-nitrobenzene gave only 41 and 37% yields respectively (Table 3, entries 12 and 13). In the case of 4-nitrobenzonitrile, standard conditions gave a mixture of 4-aminobenzonitrile and 4-nitrobenzylamine (26% and 10% respectively), while only the former was produced when KCO_2H was removed. Overall, we showed the excellent chemoselectivity of

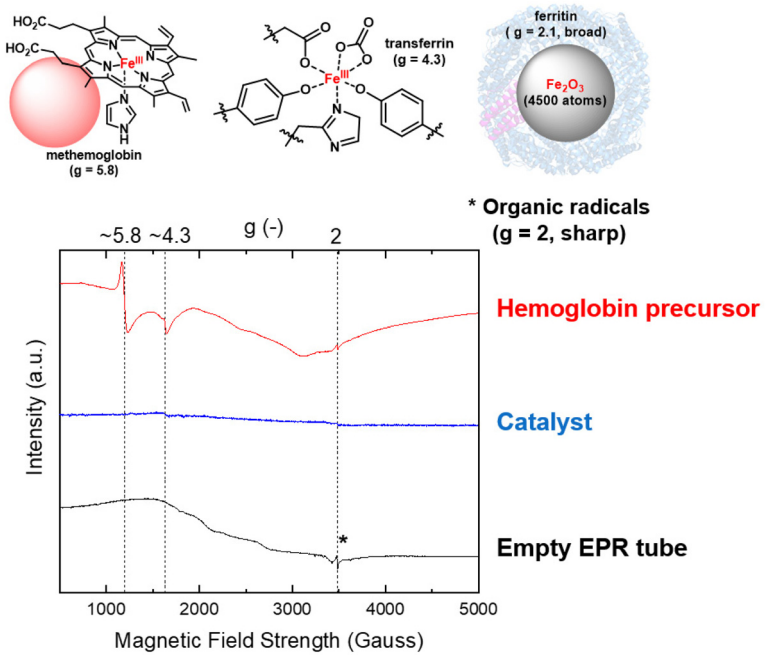

Fig. 5 X-band EPR spectrum of haemoglobin (red), FeN_x@C (blue) and empty tube (black).

Table 2 Control reactions for 4-nitrotoluene transfer hydrogenation

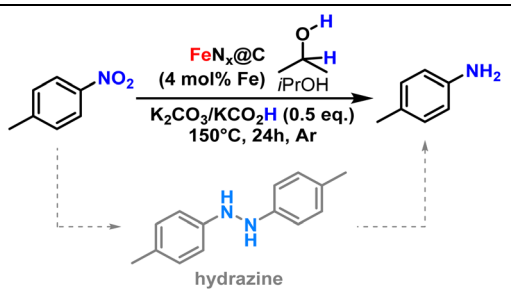

Entry	Deviation from standard conditions			Yield (%)
1	None			75
2	**Removal**	No K_2CO_3		10
3		No KCO_2H		34[a]
4		No catalyst		0
5	**Base**	Na_2CO_3		31
6		KOH		36
7		NEt_3		16
8	**Reductant**	**NH_4CO_2H**	(0.5 equiv.)	0
9			(1 equiv.)	23
10			(1.5 equiv.)	25
11	**Iron source**	**Fe^{3+}**	$FeCl_3$	0
12			$Fe(acac)_3$	0
13		**Fe^{2+}**	$FeCl_2$	14
14			FePc	0
15		**Pristine haemoglobin**		6

Standard reaction conditions: 4-nitrotoluene (12.4 mg, 88 μmol), base and additive (0.5 equiv. each), Fe source (4 mol% Fe), isopropyl alcohol (2.0 mL), Ar, 150 °C, 24 h. [a] 38% of 1,2-di-*p*-tolylhydrazine was formed.

our catalytic system can be achieved, with the exception of nitrobenzaldehydes and nitrovinyls (see ESI for details, Fig. S16†).

With this methodology, we were also able to prepare 2-phenylbenzimidazole, an important scaffold involved in anticancer drugs, in a one-pot reduction/cyclisation tandem reaction from 2-nitroaniline.[53] For this, we replaced isopropanol with benzyl alcohol, which generates an equivalent of benzaldehyde byproduct in the reduction of 2-nitroaniline into *ortho*-phenylenediamine. The two products can then undergo condensation into the desired heterocycle with 64% yield (Fig. 6).

The catalyst was easily recycled by centrifugation, and retained its activity for up to 7 cycles without a significant decrease in yield for the reduction of 4-nitrobenzene (Fig. 7).

The recovered material (after one catalytic cyle) was subjected to HAADF-STEM analysis, showing no appearance of Fe_xO_y aggregates, and we were still able to identify single-site Fe bright dots (Fig. 8, and Fig. S5–S6†), implying that the catalytic sites were retained.

Information on FeN_x coordination before and after reaction was also obtained by XAS. As shown in Fig. S12,† the Fe–K-edge X-ray absorption near-edge spectroscopy (XANES) for the catalyst before and after the reaction (FeN_x@C and FeN_x@C_{AR} respectively) is similar to that of the FePc reference sample. FeN_x@C_{AR} showed an increased pre-edge intensity (at 7113 eV), which indicates that Fe has a more symmetric coordination pattern than in FeN_x@C.[54] The Fourier transform (FT) of the extended X-ray absorption fine structure (EXAFS) spectrum for Fe-before and Fe-after samples showed a main peak at 1.5 Å and 1.4 Å (phase uncorrected), corresponding to the

Table 3 Nitroarene reduction substrate scope (reduced nitro group is highlighted in blue, and the other reducible/cleavable functional groups are highlighted in purple)

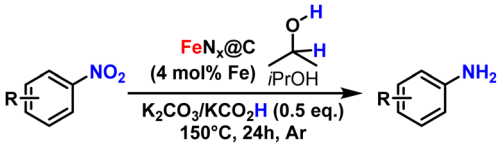

Entry	Product		Yield (%)
1	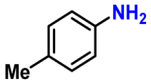		75
2	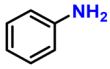		85
3	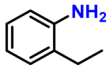		69[a]
4	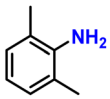		77
5	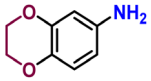		84
6	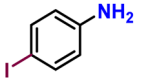		58
7	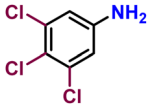		46
8	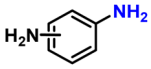	*Ortho-*	97[a]
9		*Meta-*	93[a]
10		*Para-*	57[a]
11	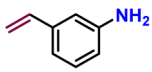		71
12	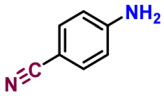		41[b]
13	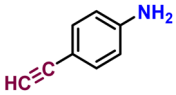		37[a]

Standard reaction conditions: nitroarene (88 μmol), K_2CO_3 (6.1 mg, 0.5 equiv.), KCO_2H (3.7 mg, 0.5 equiv.), FeN_x@C (50 mg, 4 mol% Fe), isopropyl alcohol (2.0 mL), Ar, 150 °C, 24 h. [a] 5 mol% Fe was used by adjusting substrate amount to 70 μmol. [b] KCO_2H was not added.

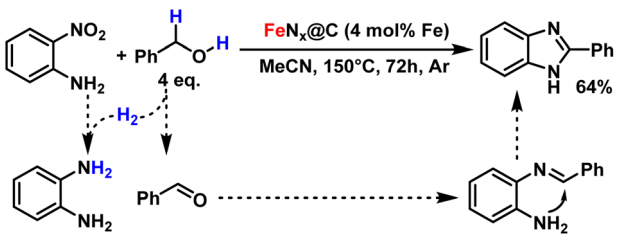

Fig. 6 One-pot preparation of 2-phenylbenzimidazole.

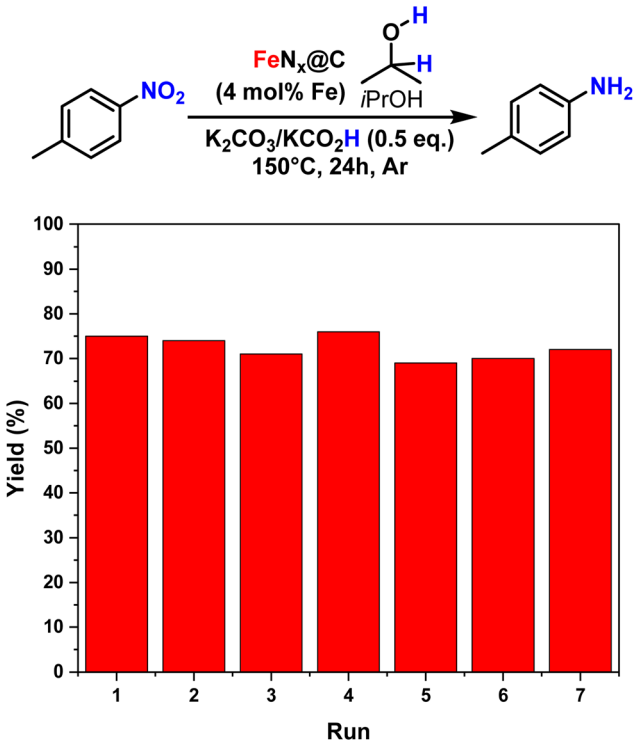

Fig. 7 Recycling of the catalyst.

first shell Fe–N or Fe–O (Fig. S12E†). The shorter first shell bond distance for FeN_x@C_{AR} suggests a change in the local coordination environment. A comparison with Zitolo *et al.*'s spectra (Fig. S14†) indicates the similarities of our samples (FeN_x@C and FeN_x@C_{AR}) with their FeN_4–O and FeN_4–O_2 samples. Together with the pre-edge features, we propose a FeN_4–O structure for FeN_x@C and FeN_4–O_2 for FeN_x@C_{AR}, respectively.[55] Wavelet transform (WT) EXAFS was employed to visualise the nearby atoms by providing the radial distance and *k* space resolutions. As shown in Fig. S15,† WT of FeN_x@C and FeN_x@C_{AR} showed one prominent peak at ~4.7 $Å^{-1}$ and 4.2 $Å^{-1}$, respectively, which is very close to that in the reference FePc (~4.2 $Å^{-1}$). Moreover, they are different from the FeO, Fe_2O_3, and Fe foil reference samples, suggesting the dominant iron species in both samples is FeN_4 sites, at least at the resolution of this experiment. Due to the similar bond distance, it is difficult to distinguish the difference between Fe–N and Fe–O in single sites. However, together with XPS, EPR, and STEM, we propose that Fe–N is the main species on the first shell.

EXAFS fittings were performed to get more insight on the coordination environment (Fig. S12†). All fittings are in good consistency with experimental data. The best fit values (Table S3†) of FeN_x@C gave an average coordination number of 4.85 for Fe–N at 2.04 Å, 2.10 for Fe–C at 2.35 Å, while the coordination number for FeN_x@C_{AR} was 5.95 for Fe–N at 1.91 Å, 2.63 for Fe–C at 2.28 Å, and 0.77 for Fe–Fe at 2.52 Å. A minor Fe–Fe peak arising from FeN_x@C_{AR} sample might originate from trace amount Fe_2O_3 from Celite used for filtration

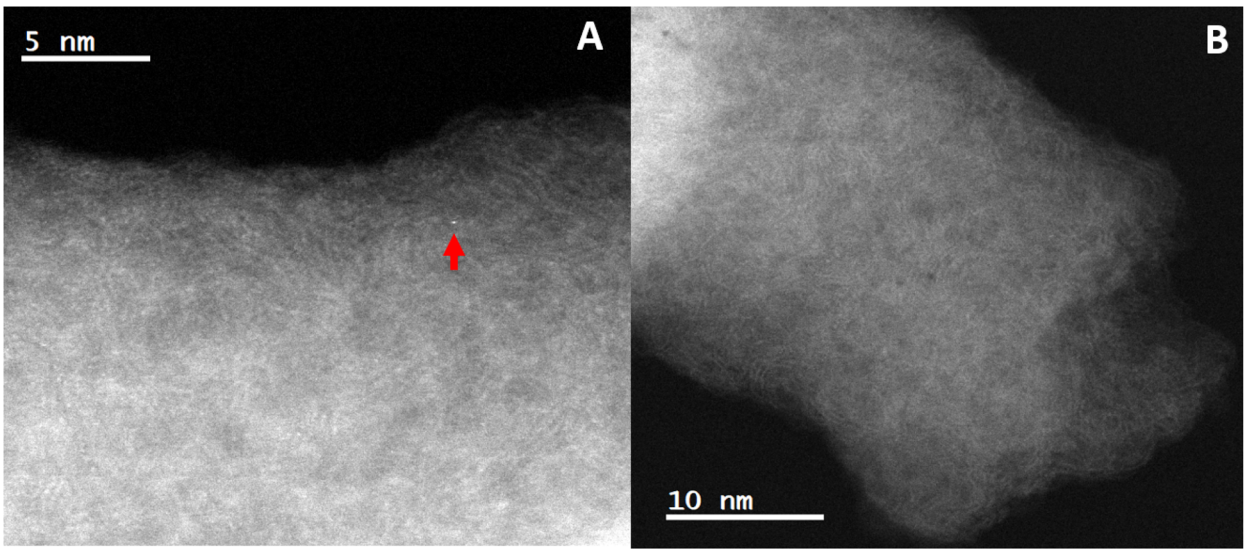

Fig. 8 (A) and (B) Post-reaction HAADF-STEM image of $FeN_x@C_{AR}$ (single site Fe are indicated with a red arrow).

or traces Fe in K_2CO_3 (see notes in ESI†).[56] As shown in Fig. S8d,† an increased coordination number and decreased bond length could be seen in the $FeN_x@C_{AR}$. Together with XANES pre-edge features, we propose a FeN_4 structure co-ordinated to one axial ligand before reaction, while $FeN_x@C_{AR}$ exhibits a FeN_4 structure coordinated to 2 axial ligands with a more symmetric structure. The nature of the axial ligand is still uncertain, although at least one is most likely an oxygen molecule, or some leftover nitrogen-containing product from the reaction.

Conclusions

In summary, we have shown for the first time the potential of haemoglobin-derived Fe catalysts for organic transformations. Unlike most reports, only biomass precursors were used (xylose and haemoglobin) and no Fe aggregation was observed, avoiding a commonly-used washing step in the preparation. Its single-site nature was demonstrated by high-end techniques (XAS, HAADF-STEM), and remained stable throughout the catalytic cycles. We have shown it to be highly selective towards a number of substrates, and active at low Fe loading (4–5 mol%), with isopropanol, K_2CO_3 and KCO_2H. We believe that this work will pave a way for pure biomass-based catalysts applied to organic reactions, while setting a high standard for single-site material characterisation for thermal catalysis.

Author contributions

A. Y. L. designed the project, prepared the materials and performed all the catalytic tests, the ICP-MS and N_2 adsorption experiments. H. L. performed the TEM/SEM images and assisted for HAADF-STEM analysis. J. F. and H. L. performed the XAS analysis. A. P. performed the EPR analysis. J. B. performed the XPS analysis. J. R. performed the Raman and the XRD analysis and helped for N_2 adsorption result interpretation. M. M. T. and K. K. H. supervised the study. The manuscript was written through contributions of all authors. All authors have given approval to the final version of the manuscript.

Conflicts of interest

There are no conflicts to declare.

Acknowledgements

The authors thank Dr Monica Amboage from the I20-EDE (SP28663) at Diamond Light Source to support and assist the X-Ray measurements, and Dr Thomas Slater from the electron Physical Science Imaging Centre (ePSIC) at Diamond Light Source to support and assist the HAADF-STEM imaging (mg28698). The authors thank as well Patricia Carry and Kaho Cheung for the use and support of the Analytical Laboratory in the Department of Chemical Engineering at Imperial College London and Gwilherm Kerherve for the use and support of the XPS suite in the Department of Materials at Imperial College London. A. P. thanks the EPSRC Centre for Doctoral Training in the Advanced Characterization of Materials (grant number EP/L015277/1) and the Imperial College London SPIN-Lab (equipment grant number: EP/P030548/1). A. Y. L. acknowledges Marie Skłodowska-Curie Fellowship H2020-MSCA-IF-2019 (892614) through the project HAEMOGLOBIN. M. M. T. acknowledges the Royal Academy of Engineering Chair in Emerging Technologies Fellowship. We thank Dr Servann Herou for his priceless advice and training, and Mengnan Wang for handling the elemental analysis of the catalyst.

References

1 B. Amini and S. Lowenkron, in *Kirk–Othmer Encyclopedia of Chemical Technology*, John Wiley & Sons, Ltd, 2003.
2 K. Weissermel and H.-J. Arpe, *Industrial Organic Chemistry, 3rd, Completely Revised Edition*, 2008.
3 A. Corma and P. Serna, *Science*, 2006, **313**, 332 LP–332334.
4 P. Serna and A. Corma, *ACS Catal.*, 2015, **5**, 7114–7121.
5 J. Song, Z.-F. Huang, L. Pan, K. Li, X. Zhang, L. Wang and J.-J. Zou, *Appl. Catal., B*, 2018, **227**, 386–408.
6 D. Formenti, F. Ferretti, F. K. Scharnagl and M. Beller, *Chem. Rev.*, 2019, **119**, 2611–2680.
7 H. Niu, J. Lu, J. Song, L. Pan, X. Zhang, L. Wang and J.-J. Zou, *Ind. Eng. Chem. Res.*, 2016, **55**, 8527–8533.
8 G. Wienhöfer, M. Baseda-Krüger, C. Ziebart, F. A. Westerhaus, W. Baumann, R. Jackstell, K. Junge and M. Beller, *Chem. Commun.*, 2013, **49**, 9089–9091.
9 S. Enthaler, K. Junge and M. Beller, *Angew. Chem., Int. Ed.*, 2008, **47**, 3317–3321.
10 A. Li, S. A. Nicolae, M. Qiao, K. Preuss, P. A. Szilágyi, A. Moores and M.-M. Titirici, *ChemCatChem*, 2019, **11**, 3602–3625.
11 R. V. Jagadeesh, A.-E. Surkus, H. Junge, M.-M. Pohl, J. Radnik, J. Rabeah, H. Huan, V. Schünemann, A. Brückner and M. Beller, *Science*, 2013, **342**, 1073–1076.
12 R. V. Jagadeesh, T. Stemmler, A.-E. Surkus, H. Junge, K. Junge and M. Beller, *Nat. Protoc.*, 2015, **10**, 548.
13 R. v. Jagadeesh, G. Wienhöfer, F. A. Westerhaus, A.-E. Surkus, M.-M. Pohl, H. Junge, K. Junge and M. Beller, *Chem. Commun.*, 2011, **47**, 10972–10974.
14 L. Liu, B. Wang, R. Gao, D. Zhang, W. Xu, L. Chen, X. Yan and Y. Li, *RSC Adv.*, 2020, **10**, 10689–10694.
15 R. v. Jagadeesh, K. Natte, H. Junge and M. Beller, *ACS Catal.*, 2015, **5**, 1526–1529.
16 P. Veerakumar, I. Panneer Muthuselvam, C.-T. Hung, K.-C. Lin, F.-C. Chou and S.-B. Liu, *ACS Sustainable Chem. Eng.*, 2016, **4**, 6772–6782.
17 O. Beswick, I. Yuranov, D. T. L. Alexander and L. Kiwi-Minsker, *Catal. Today*, 2015, **249**, 45–51.
18 X. Cui, Q. Zhang, M. Tian and Z. Dong, *New J. Chem.*, 2017, **41**, 10165–10173.
19 X.-F. Yang, A. Wang, B. Qiao, J. Li, J. Liu and T. Zhang, *Acc. Chem. Res.*, 2013, **46**, 1740–1748.
20 H. Jin, P. Li, P. Cui, J. Shi, W. Zhou, X. Yu, W. Song and C. Cao, *Nat. Commun.*, 2022, **13**, 723.
21 H.-Y. Zhuo, X. Yu, Q. Yu, H. Xiao, X. Zhang and J. Li, *Sci. China Mater.*, 2020, **63**, 1741–1749.
22 Q. Shen, H. Jin, P. Li, X. Yu, L. Zheng, W. Song and C. Cao, *Nano Res.*, 2022, **15**, 5024–5031.
23 G. Lu, K. Sun, Y. Lin, Q. Du, J. Zhang, K. Wang and P. Wang, *Nano Res.*, 2022, **15**, 603–611.
24 W.-C. Cheong, W. Yang, J. Zhang, Y. Li, D. Zhao, S. Liu, K. Wu, Q. Liu, C. Zhang, D. Wang, Q. Peng, C. Chen and Y. Li, *ACS Appl. Mater. Interfaces*, 2019, **11**, 33819–33824.
25 R. Yun, F. Zhan, N. Li, B. Zhang, W. Ma, L. Hong, T. Sheng, L. Du, B. Zheng and S. Liu, *ACS Appl. Mater. Interfaces*, 2020, **12**, 34122–34129.
26 J. Maruyama and I. Abe, *Chem. Mater.*, 2005, **17**, 4660–4667.
27 J. Maruyama and I. Abe, *Chem. Mater.*, 2006, **18**, 1303–1311.
28 J. Maruyama, J. Okamura, K. Miyazaki and I. Abe, *J. Phys. Chem. C*, 2007, **111**, 6597–6600.
29 J. Maruyama, J. Okamura, K. Miyazaki, Y. Uchimoto and I. Abe, *J. Phys. Chem. C*, 2008, **112**, 2784–2790.
30 W. Chen, X. Luo, S. Ling, Y. Zhou, B. Shen, T. J. A. Slater, J. A. Fernandes, T. Lin, J. Wang and Y. Shen, *Carbon*, 2020, **168**, 588–596.
31 C.-Z. Guo, C.-G. Chen and Z.-L. Luo, *J. Power Sources*, 2014, **245**, 841–845.
32 J. Maruyama, T. Hasegawa, T. Amano, Y. Muramatsu, E. M. Gullikson, Y. Orikasa and Y. Uchimoto, *ACS Appl. Mater. Interfaces*, 2011, **3**, 4837–4843.
33 J. Maruyama, T. Hasegawa, S. Iwasaki, H. Kanda and H. Kishimoto, *ACS Sustainable Chem. Eng.*, 2014, **2**, 493–499.
34 X. Li, Y. Chen and J. Nielsen, *Curr. Opin. Biotechnol*, 2019, **57**, 56–65.
35 Y. Gong, Z. Wei, J. Wang, P. Zhang, H. Li and Y. Wang, *Sci. Rep.*, 2014, **4**, 6349.
36 M.-M. Titirici and M. Antonietti, *Chem. Soc. Rev.*, 2010, **39**, 103–116.
37 S. A. Nicolae, H. Au, P. Modugno, H. Luo, A. E. Szego, M. Qiao, L. Li, W. Yin, H. J. Heeres, N. Berge and M.-M. Titirici, *Green Chem.*, 2020, **22**, 4747–4800.
38 K. Preuss, L. C. Tănase, C. M. Teodorescu, I. Abrahams and M.-M. Titirici, *J. Mater. Chem. A*, 2017, **5**, 16336–16343.
39 N. Baccile, M. Antonietti and M.-M. Titirici, *ChemSusChem*, 2010, **3**, 246–253.
40 M. Paneque, J. M. de la Rosa, J. Kern, M. T. Reza and H. Knicker, *J. Anal. Appl. Pyrolysis*, 2017, **128**, 314–323.
41 M. C. Martins Alves and G. Tourillon, *J. Phys. Chem.*, 1996, **100**, 7566–7572.
42 W. R. Hagen, *Dalton Trans.*, 2006, 4415–4434.
43 L. Ni, C. Gallenkamp, S. Paul, M. Kübler, P. Theis, S. Chabbra, K. Hofmann, E. Bill, A. Schnegg, B. Albert, V. Krewald and U. I. Kramm, *Adv. EnergySustain. Res.*, 2021, **2**, 2000064.
44 M. M. Roessler and E. Salvadori, *Chem. Soc. Rev.*, 2018, **47**, 2534–2553.
45 S. Gladiali and E. Alberico, *Chem. Soc. Rev.*, 2006, **35**, 226–236.
46 P. E. Sues, K. Z. Demmans and R. H. Morris, *Dalton Trans.*, 2014, **43**, 7650–7667.
47 G. Wienhöfer, I. Sorribes, A. Boddien, F. Westerhaus, K. Junge, H. Junge, R. Llusar and M. Beller, *J. Am. Chem. Soc.*, 2011, **133**, 12875–12879.
48 K. Junge, B. Wendt, N. Shaikh and M. Beller, *Chem. Commun.*, 2010, **46**, 1769–1771.

49 K. J. Datta, A. K. Rathi, M. B. Gawande, V. Ranc, G. Zoppellaro, R. S. Varma and R. Zboril, *ChemCatChem*, 2016, **8**, 2351–2355.
50 H. Wiener, J. Blum and Y. Sasson, *J. Org. Chem.*, 1991, **56**, 4481–4486.
51 F. Ghani, J. Kristen and H. Riegler, *J. Chem. Eng. Data*, 2012, **57**, 439–449.
52 H.-U. Blaser, H. Steiner and M. Studer, *ChemCatChem*, 2009, **1**, 210–221.
53 S. Yadav, B. Narasimhan and H. kaur, *Adv. Anticancer Agents Med. Chem.*, 2016, **16**, 1403–1425.
54 X. Xie, C. He, B. Li, Y. He, D. A. Cullen, E. C. Wegener, A. J. Kropf, U. Martinez, Y. Cheng, M. H. Engelhard, M. E. Bowden, M. Song, T. Lemmon, X. S. Li, Z. Nie, J. Liu, D. J. Myers, P. Zelenay, G. Wang, G. Wu, V. Ramani and Y. Shao, *Nat. Catal.*, 2020, **3**, 1044–1054.
55 A. Zitolo, V. Goellner, V. Armel, M.-T. Sougrati, T. Mineva, L. Stievano, E. Fonda and F. Jaouen, *Nat. Mater.*, 2015, **14**, 937–942.
56 Imerys filtration, Celite specification sheet, **https://nika-iv.com/en/diatomite/tds/FR_C_574.pdf**, (accessed 2 December 2021).